Non-Similar Computational Solution for Boundary Layer Flows of Non-Newtonian Fluid from an Inclined Plate with Thermal Slip

A. Subba Rao[1†], V. Ramachandra Prasad[1], N. Nagendra[1], N. Bhaskar Reddy[2] and O. Anwar Beg[3]

[1] *Department of Mathematics, Madanapalle Institute of Technology and Science, Madanapalle-517325, India.*
[2] *Department of Mathematics, Sri Venkateswara University, Tirupathi-517502, Andrapradesh, India.*
[3]*Gort Engovation Research (Propulsion and Biomechanics),15 Southmere Avenue, Bradford, WestYorkshire BD73NU,UK.*

†*Corresponding Author Email: asrsvu@gmail.com*

ABSTRACT

The laminar boundary layer flow and heat transfer of Casson non-Newtonian fluid from an inclined (solar collector) plate in the presence of thermal and hydrodynamic slip conditions is analysed. The inclined plate surface is maintained at a constant temperature. The boundary layer conservation equations, which are parabolic in nature, are normalized into *non-similar* form and then solved numerically with the well-tested, efficient, implicit, stable Keller-box finite-difference scheme. Increasing velocity slip induces acceleration in the flow near the inclined plate surface. Increasing velocity slip consistently enhances temperatures throughout the boundary layer regime. An increase in thermal slip parameter strongly decelerates the flow and also reduces temperatures in the boundary layer regime. An increase in Casson rheological parameter acts to elevate considerably the velocity and this effect is pronounced at higher values of tangential coordinate. Temperatures are however very slightly decreased with increasing values of Casson rheological parameter.

NOMENCLATURE

C_f	skin friction coefficient	α	thermal diffusivity
S_f	non-dimensional velocity slip parameter	β	non-Newtonian (rheological) Casson parameter
S_T	non-dimensional thermal slip parameter		
f	non-dimensional steam function	η	dimensionless radial coordinate
g	acceleration due to gravity	μ	dynamic viscosity
Gr	Grashof number		
N_0	velocity slip factor	ν	kinematic viscosity
K_0	thermal slip factor	θ	non-dimensional temperature
Nu	Local Nusselt number	ρ	density of fluid
Pr	Prandtl number	ξ	dimensionless tangential coordinate
T	temperature	ψ	dimensionless stream function
u, v	non-dimensional velocity components along the x- and y directions, respectively		
x, y	non-dimensional Cartesian coordinates along and transverse to plate surface		

Subscripts

w	conditions on the wall
∞	free stream conditions

1. INTRODUCTION

The heat transfer from inclined surfaces finds numerous applications in solar energy systems, geophysics, materials processing etc. Many studies have appeared concerning natural and also mixed

convection flows. Kierkus (1968) studied isothermal inclined plate natural convection boundary layer flow using a perturbation method for a Prandtl number of 0.7. Fujii and Imura (1972) studied experimentally free convection from an inclined plate. Chen *et al.* (1980) analyzed combined heat and mass transfer in mixed convection along vertical inclined plates. Uniform surface flux effects on inclined plate thermal convection were reported by Armaly *et al.* (1987). The combined buoyancy and wall transpiration effects on mixed convection along an inclined plate were studied by Lee and Hsu (1989). Wickern (1991) examined the laminar boundary layer flow over an arbitrarily sloping plate showing that for opposing buoyancy forces singular as well as regular behaviour may prevail. Further studies have been communicated by Yan and Soong (1995) in the context of evaporating inclined boundary layer convection and by Sheu and Lin (1996) in combusting inclined flat plate flows.

Non-Newtonian transport phenomena arise in many branches of process mechanical, chemical and materials engineering. Such fluids exhibit shear-stress-strain relationships which diverge significantly from the classical Newtonian (Navier-Stokes) model. Most non-Newtonian models involve some form of modification to the momentum conservation equations. These include power-law fluids (O. Anwar Bég, 2012), viscoelastic fluids including Maxwell upper-convected models (O. Anwar Bég, 2011a), Oldroyd-B models (Tripathi, 2012), differential Reiner-Rivlin models (M.M. Rashidi *et.al*, 2012) and Bingham plastics (R.P. Chhabra, 2014). The flow of non-Newtonian fluids in the presence of heat transfer is an important research area due to its relevance to the foodstuffs (Steffe, 2001). Of the various rheological models developed in biotechnology and food engineering, the Casson model has proved very successful. This simple, yet elegant rheological model was introduced originally (Casson, 1959) to simulate industrial inks. This model (Bird, 1983) constitutes a plastic fluid model which exhibits shear thinning characteristics, yield stress and high shear viscosity. The Casson fluid model is reduced to a Newtonian fluid at a very high wall shear stress i.e. when the wall stress is much greater than yield stress. This fluid model also approximates reasonably well the rheological behaviour of other liquids including physiological suspensions, foams, cosmetics, syrups etc.

A number of theoretical, numerical and experimental studies of transport phenomena in Casson fluids have been presented in a variety of areas including biomedical engineering (R. K. Dash,2000) and manufacturing technology (Batra,1992). Neofytou (2006) studied computationally the flow characteristics of both power-law and Casson fluids in symmetric sudden expansions, showing that the critical generalized Reynolds number of transition from symmetry to asymmetry and subsequently the inverse dimensionless wall shear stress are linearly related to the dimensionless wall shear rate.

Hemodynamic simulations of Casson blood flow in complex arterial geometries were studied by Gorla *et al.* (2009) and Murthy and Pradhan (2010). Attia and Sayed-Ahmed (2010) studied the unsteady hydromagnetic Couette flow and heat transfer in a Casson fluid using the Crank-Nicolson implicit method, showing that Casson number (dimensionless yield stress parameter) controls strongly the velocity overshoot and has a significant effect on the time at which the overshoot arises. Hayat *et al.* (2012) obtained homotopic solutions for stagnation-point flow and heat transfer of a Casson fluid along a stretching surface, also considering viscous heating effects.

The above studies invariably assumed the "no-slip" condition at the boundary. Slip effects have however shown to be significant in certain industrial thermal problems and manufacturing fluid dynamics systems. Sparrow *et al.* (1962) presented the first significant investigation of laminar slip-flow heat transfer for tubes with uniform heat flux. Inman (1964) further described the thermal convective slip flow in a parallel plate channel or a circular tube with uniform wall temperature. These studies generally indicated that velocity slip acts to enhance heat transfer whereas thermal slip depresses heat transfer.

Many studies have appeared in recent years considering both hydrodynamic and thermal slip effects. Interesting articles of relevance to process mechanical engineering include Larrode *et al.* (2000) who studied thermal/velocity slip effects in conduit thermal convection. Studies of slip flows from curved bodies include Bég *et al.* (2011b) who examined using network numerical simulation the magneto-convective slip flow from a rotating disk, Wang and Ng (2011) who studied using asymptotic analysis the slip hydrodynamics from a stretching inclined plate. Wang (2007) has also examined stagnation slip flow and heat transfer from an axially moving inclined plate showing that heat transfer increases with slip, Prandtl number and Reynolds number, and that in the case of large slip, the flow field decays exponentially into potential flow.

The objective of the present work is to investigate the influence of the inclination of the plate on the mixed convection heat transfer of a Casson rheological fluid past an inclined plate (solar energy collector) system using boundary layer theory. The effects of governing thermo physical parameters on heat transfer characteristics are analysed in detail. Mathematical modelling through equations of continuity and motion leads to dimensionless nonlinear coupled differential boundary layer equations. The velocity and thermal slip conditions along with conservation law of mass, momentum and energy completes the problems formulation for velocity components and temperature. A finite difference numerical solution is presented for the transformed boundary layer equations and a parametric study is conducted the Prandtl number, Casson rheological parameter, wall suction/injection and velocity/thermal slip effects on the momentum and heat transfer characteristics

conducted. The present problem has to the authors' knowledge not appeared thus far in the scientific literature.

2. MATHEMATICAL FLOW MODEL

Consider the combined thermal convection and diffusion mass transfer in laminar boundary layer flow parallel to a flat plate which is inclined to the vertical with angle, γ, with free stream velocity, u_∞, as depicted in Figure 1. The temperature of the ambient medium is T_∞ and wall temperature is T_w. The flow along the plate contains a species, A, slightly soluble in the fluid. The stream wise coordinate, *x*, is measured from the leading edge of the plate, parallel to the plate and the transverse coordinate, *y*, normal to the plate in the outward direction, for flow regimes both above and beneath the plate.

The forced flow, following Beg *et al.* (2011c) exists the plate for $\gamma > 0$ in the clockwise direction and beneath the plate for $\gamma < 0$ (in the anti-clockwise direction). The fluid properties are assumed to be constant except the density variation in the buoyancy force term.
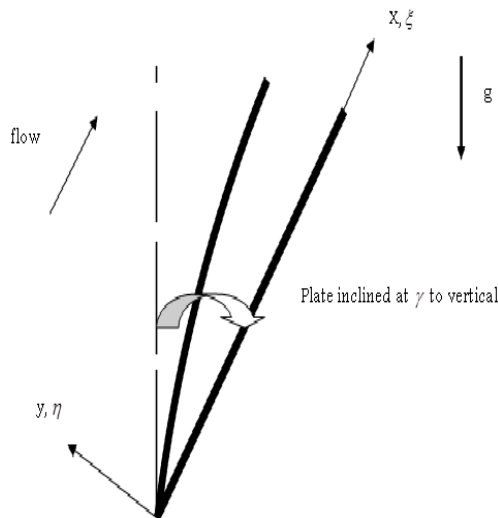

Fig. 1. Physical Model and Coordinate System.

The rheological equation of state for an isotropic flow of Casson fluid, following Steffe (2001) in tensorial notation may be stated as:

$$\tau_{ij} = \begin{cases} 2\left(\mu_B + \dfrac{p_y}{\sqrt{2\pi}}\right)e_{ij}, \pi \ge \pi_c \\ 2\left(\mu_B + \dfrac{p_y}{\sqrt{2\pi_c}}\right)e_{ij}, \pi < \pi_c \end{cases} \tag{1}$$

in which $\pi = e_{ij}e_{ij}$ and e_{ij} is the $(i,j)^{th}$ component of deformation rate, π denotes the product of the component of deformation rate with itself, π_c shows a critical value of this product based on

the non-Newtonian model, μ_B the plastic dynamic viscosity of non-Newtonian fluid and p_y is the yield stress of fluid. Introducing the boundary layer approximations, the governing conservation equations can be written as follows:

$$\frac{\partial u}{\partial x} + \frac{\partial v}{\partial y} = 0 \tag{2}$$

$$u\frac{\partial u}{\partial x} + v\frac{\partial u}{\partial y} = \pm g\Lambda Sin\gamma \frac{\partial}{\partial x}\int_y^\infty (T-T_\infty)dy$$

$$\pm g\Lambda(T-T_\infty)Cos\gamma + \nu\left(1+\frac{1}{\beta}\right)\frac{\partial^2 u}{\partial y^2} \tag{3}$$

$$u\frac{\partial T}{\partial x} + v\frac{\partial T}{\partial y} = \alpha\frac{\partial^2 T}{\partial y^2} \tag{4}$$

The first term on the RHS of Equation (3) correspond to the stream wise pressure gradients induced by the combined buoyancy forces, with the plus and the minus signs representing, respectively, flows above and below the plate. The second term corresponds to the buoyancy forces generated by thermal and mass diffusion, with the plus and minus signs referring, respectively, to upward and downward forced flows. The final term in (3) on the right hand side is the viscous diffusion term. The initial and boundary conditions at the plate and in the free stream are:

$$u = u_\infty, T = T_\infty \quad at \quad x = 0$$

$$\left.\begin{cases} u = u_\infty + N_0\left(1+\dfrac{1}{\beta}\right)\dfrac{\partial u}{\partial y}, \\ v = -V_w, \quad T = T_w + K_0\dfrac{\partial T}{\partial y} \end{cases}\right\} \quad at \quad y = 0 \tag{5}$$

$$u \to u_\infty, \ T \to T_\infty \ as \ y \to \infty$$

In which N_0 is the velocity slip factor and K_0 is the thermal slip factor. For $N_0=0=K_0$, one can recover the classical no-slip case. where u and v denote the velocity components in the x- and y-directions respectively, ν is the kinematic viscosity, Λ is the coefficients of thermal expansion , respectively, T is the temperature ,respectively, ρ is the density, C_p is the specific heat capacity, α is the thermal diffusivity, T_m is the mean fluid temperature. Also, as indicated by Beg *et al.* (2011c), Equation (3) indicates the existence of both buoyancy induced stream wise pressure gradient terms and the buoyancy force terms for an inclined surface. The relative magnitude of these terms, however is controlled by the angle of inclination of the plate to the vertical, γ. Chen *et al.* (1980) have shown using an order- of-magnitude analysis that the buoyancy-induced stream wise pressure gradient terms can be neglected in comparison with the buoyancy force terms provided:

$$\frac{\delta}{x}Tan\gamma \ll 1 \tag{6}$$

Chen *et al.* (1980) have further shown that in terms of dimensionless boundary layer thickness η_δ (the η value for which $y = \delta$), the condition (6) is also equivalent to the following condition:

$$Tan\gamma \ll \frac{\mathrm{Re}_x^{1/2}}{\eta_\delta} \tag{7}$$

Where $\mathrm{Re}_x = u_\infty x / \nu$ denotes the local Reynolds number. Effectively the condition (6) or (7) is valid for $Tan\gamma \ll 3 \sim 30$ i.e. angles of inclination, $\gamma \ll 72 \sim 88$ degrees. In this situation, the buoyancy-induced stream wise pressure gradient terms are omitted in Equation (3) which reduces to the much simpler form:

$$u\frac{\partial u}{\partial x} + v\frac{\partial u}{\partial y} = \pm g\Lambda(T - T_\infty)Cos\gamma + \nu\left(1 + \frac{1}{\beta}\right)\frac{\partial^2 u}{\partial y^2} \tag{8}$$

The governing boundary layer equations then comprise Equations (2)-(4) and (8), with boundary conditions (5) subject to the condition given by (6) and (7). The special case of a vertical plate is retrieved from (8) for $\gamma = 0^0$ *i.e.* $\cos\gamma = 1$. Proceeding with the analysis we introduce the following dimensionless variables:

$$\eta = y\left(\frac{u_\infty}{\nu x}\right)^{1/2},$$

$$\xi = \xi(x) \ , \ f(\xi,\eta) = \frac{\psi(x,y)}{(\nu u_\infty x)^{1/2}} \ ,$$

$$Gr = \frac{g\Omega(T_w - T_\infty)x^3}{\nu^2},$$

$$\beta = \mu_B \frac{\sqrt{2\pi_c}}{p_y}, \quad \theta(\xi,\eta) = \frac{T - T_\infty}{T_w - T_\infty} \tag{9}$$

Where η the pseudo-similarity is variable, ξ is transformed *x*-coordinate which represents the thermal buoyancy effects, β - is the non-Newtonian Casson parameter, f is a reduced stream function, θ is dimensionless temperature. Where T_∞ - the free stream temperature, V_w - the uniform blowing/suction velocity. The stream function $\psi(x,y)$ satisfies the mass conservation equation (3) with

$$u = \frac{\partial\psi}{\partial y} \ , \qquad v = -\frac{\partial\psi}{\partial x}$$

In view of Equation (6), Equations (2) - (4) reduce to the following coupled, nonlinear, dimensionless partial differential equations for momentum and energy for the regime:

$$\left(1 + \frac{1}{\beta}\right)f''' + \frac{1}{2}ff'' + \xi\theta\cos\gamma = \xi\left(f'\frac{\partial f'}{\partial\xi} - f''\frac{\partial f}{\partial\xi}\right) \tag{10}$$

$$\frac{\theta''}{\mathrm{Pr}} + \frac{1}{2}f\theta' = \xi\left(f'\frac{\partial\theta}{\partial\xi} - \theta'\frac{\partial f}{\partial\xi}\right) \tag{11}$$

The transformed dimensionless boundary conditions are:

At $\eta = 0, \quad f = S, \quad f' = \left(1 + \frac{1}{\beta}\right)S_f f''(0), \quad \theta = 1 + S_T\theta'(0)$

As $\quad \eta \to \infty \qquad f' \to 1, \ \theta \to 0 \tag{12}$

In the above equations, the primes denote the differentiation with respect to η, Pr is the Prandtl number, the thermal buoyancy force parameter, $\xi = \frac{Gr_x}{\mathrm{Re}_x^2}$ (which is a measure of thermal buoyancy force effect on forced convection), $S_f = \frac{N_0\mathrm{Re}_x^{1/2}}{x}$ and $S_T = \frac{K_0\mathrm{Re}_x^{1/2}}{x}$ are the non-dimensional velocity slip and thermal slip parameters respectively and f_w is the blowing/suction parameter. $f_w < 0$ for $V_w > 0$ (the case of blowing), and $f_w > 0$ for $V_w < 0$ (the case of suction). Of course the special case of a solid inclined plate surface corresponds to fw = 0. Here we assumed the typical values $K_0 = 0.5$, $N_0 = 0.25$ for finding the non-dimensional velocity and thermal slip parameters.

The engineering design quantities of physical interest include the skin-friction coefficient and Nusselt number, which are given by:

$$\frac{1}{2}C_f\mathrm{Re}_x^{1/2} = \left(1 + \frac{1}{\beta}\right)f''(\xi,0) \tag{13}$$

$$N_u\mathrm{Re}_x^{-1/2} = -\theta'(\xi,0) \tag{14}$$

3. NUMERICAL SOLUTION

In this study, the efficient Keller-Box implicit difference method has been employed to solve the general flow model defined by equations (10) – (11) with boundary conditions (12). This method was originally developed for low speed aerodynamic boundary layers by Keller (1970), and has been employed in a diverse range of industrial multi-physical fluid dynamics problems. These include cross-diffusion boundary layer flows (Prasad et.al, 2011b). The fundamental phases intrinsic to the Keller Box Scheme are:

a. Reduction of the Nth order partial differential equation system to N first order equations

b. Finite Difference Discretization

c. Quasilinearization of Non-Linear Keller Algebraic Equations

d. Block-tridiagonal Elimination of Linear Keller Algebraic Equations

Phase a: *Reduction of the Nth order partial*

differential equation system to N first order equations

Equations (10) – (11) subject to the boundary conditions (12) are first written as a system of first-order equations.
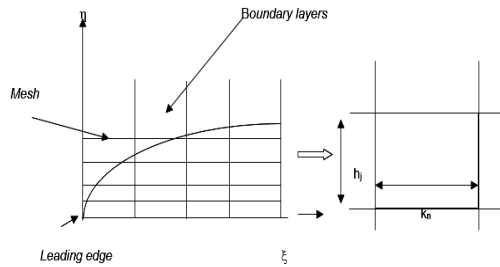

Fig. 2. Grid Meshing and a Keller Box Computational Cell.

For this purpose, we reset Eqns. (10) – (11) as a set of simultaneous equations by introducing the new variables *u, v* and *t*:

$$f' = u \tag{15}$$

$$f'' = v \tag{16}$$

$$\theta' = t \tag{17}$$

$$\left(1 + \frac{1}{\beta}\right) v' + \frac{1}{2} f v + \xi \cos\gamma(s) = \xi\left(u \frac{\partial u}{\partial \xi} - v \frac{\partial f}{\partial \xi}\right) \tag{18}$$

$$\frac{t'}{\mathrm{Pr}} + \frac{1}{2} f t = \xi\left(u \frac{\partial s}{\partial \xi} - t \frac{\partial f}{\partial \xi}\right) \tag{19}$$

In terms of the dependent variables, the boundary conditions become:

$$At\ \eta = 0:\ u = \left(1 + \frac{1}{\beta}\right) f''(0),\ f = f_w,\ s = 1$$
$$As\ \eta \to \infty:\ u \to 1,\ s \to 0 \tag{20}$$

Phase b: *Finite Difference Discretization*

A two dimensional computational grid is imposed on the *ξ-η* plane as sketched in Fig. 2. The stepping process is defined by:

$$\eta_0 = 0, \quad \eta_j = \eta_{j-1} + h_j, \quad j = 1, 2, ..., J, \quad \eta_J \equiv \eta_\infty \tag{21}$$

$$\xi^0 = 0, \quad \xi^n = \xi^{n-1} + k_n, \quad n = 1, 2, ..., N \tag{22}$$

where k_n and h_j denote the step distances in the *ξ* and *η* directions respectively.

If g_j^n denotes the value of any variable at (η_j, ξ^n), then the variables and derivatives of Equations. (15) – (19) at $(\eta_{j-1/2}, \xi^{n-1/2})$ are replaced by:

$$g_{j-1/2}^{n-1/2} = \frac{1}{4}\left(g_j^n + g_{j-1}^n + g_j^{n-1} + g_{j-1}^{n-1}\right), \tag{23}$$

$$\left(\frac{\partial g}{\partial \eta}\right)_{j-1/2}^{n-1/2} = \frac{1}{2h_j}\left(g_j^n - g_{j-1}^n + g_j^{n-1} - g_{j-1}^{n-1}\right), \tag{24}$$

$$\left(\frac{\partial g}{\partial \xi}\right)_{j-1/2}^{n-1/2} = \frac{1}{2k^n}\left(g_j^n - g_{j-1}^n + g_j^{n-1} - g_{j-1}^{n-1}\right), \tag{25}$$

We now state the finite-difference approximation of equations. (15) – (19) for the *mid-point* $\left(\eta_{j-1/2}, \xi^n\right)$, below

$$h_j^{-1}\left(f_j^n - f_{j-1}^n\right) = u_{j-1/2}^n, \tag{26}$$

$$h_j^{-1}\left(u_j^n - u_{j-1}^n\right) = v_{j-1/2}^n, \tag{27}$$

$$\left(1 + \frac{1}{\beta}\right)\left(v_j - v_{j-1}\right)$$
$$+ \frac{(1 + 2\alpha)h_j}{8}\left[\left(f_j + f_{j-1}\right)\left(v_j + v_{j-1}\right)\right]$$
$$- \frac{\alpha h_j}{4}\left(u_j + u_{j-1}\right)^2 + \frac{1}{2}\xi h_j \cos\gamma\left(s_j + s_{j-1}\right)$$
$$+ \frac{\alpha h_j}{2} v_{j-1/2}^{n-1}\left(f_j + f_{j-1}\right)$$
$$- \frac{\alpha h_j}{2} f_{j-1/2}^{n-1}\left(v_j + v_{j-1}\right) = \left[R_1\right]_{j-1/2}^{n-1} \tag{28}$$

$$h_j^{-1}\left(\theta_j^n - \theta_{j-1}^n\right) = t_{j-1/2}^n \tag{29}$$

$$\frac{1}{\mathrm{Pr}}\left(t_j - t_{j-1}\right) + \frac{(1 + 2\alpha)h_j}{8}\left[\left(f_j + f_{j-1}\right)\left(t_j + t_{j-1}\right)\right]$$
$$- \frac{\alpha h_j}{4}\left[\left(u_j + u_{j-1}\right)\left(s_j + s_{j-1}\right)\right]$$
$$+ \frac{\alpha h_j}{2} s_{j-1/2}^{n-1}\left(u_j + u_{j-1}\right)$$
$$- \frac{\alpha h_j}{2} u_{j-1/2}^{n-1}\left(s_j + s_{j-1}\right) - \frac{\alpha h_j}{2} f_{j-1/2}^{n-1}\left(t_j + t_{j-1}\right)$$
$$+ \frac{\alpha h_j}{2} t_{j-1/2}^{n-1}\left(f_j + f_{j-1}\right) = \left[R_2\right]_{j-1/2}^{n-1} \tag{30}$$

where we have used the abbreviations

$$\alpha = \frac{\xi^{n-1/2}}{k_n} \tag{31}$$

$$\left[R_1\right]_{j-1/2}^{n-1} = -h_j\left[\begin{array}{c}\left(1 + \frac{1}{\beta}\right)\left(\frac{v_j - v_{j-1}}{h_j}\right) + \left(\frac{1 - 2\alpha}{2}\right)\left(f_{j-1/2}v_{j-1/2}\right) \\ -\alpha\left(u_{j-1/2}\right)^2 + \xi\cos\gamma\left(s_{j-1/2}\right)\end{array}\right] \tag{32}$$

$$\left[R_2\right]_{j-1/2}^{n-1} = -h_j \left[\begin{array}{c} \dfrac{1}{\Pr}\left(\dfrac{t_j - t_{j-1}}{h_j}\right) + \left(\dfrac{1-2\alpha}{2}\right)\left(f_{j-1/2}t_{j-1/2}\right) \\[3mm] + \alpha\left(u_{j-1/2}s_{j-1/2}\right) \end{array}\right]$$

(33)

The boundary conditions are

$$f_0^n = u_0^n = 0, \theta_0^n = 1, u_J^n = 1, \theta_J^n = 0 \qquad (34)$$

Phase c: *Quasilinearization of Non-Linear Keller Algebraic Equations*

If we assume $f_j^{n-1}, u_j^{n-1}, v_j^{n-1}, s_j^{n-1}, t_j^{n-1}$ to be known for $0 \le j \le J$, Equations (26) – (30) are a system of *5J+5* equations for the solution of *5J+5* unknowns $f_j^n, u_j^n, v_j^n, s_j^n, t_j^n, j = 0, 1, 2 ..., J$. This non-linear system of algebraic equations is linearized by means of Newton's method as explained in (Keller, 1970; Prasad et.al, 2012, Prasad et.al, 2013).

Phase d: *Block-tridiagonal Elimination of Linear Keller Algebraic Equations*

The linear system (26) – (30) can now be solved by the block-elimination method, since they possess a block-tridiagonal structure. Commonly, the block-tridiagonal structure consists of variables or constants, but here, an interesting feature can be observed, namely that it consists of block matrices. The complete linearized system is formulated as a block matrix system, where each element in the coefficient matrix is a matrix itself. Then, this system is solved using the efficient Keller-box method. The numerical results are affected by the number of mesh points in both directions. After some trials in the η-direction (radial coordinate) a larger number of mesh points are selected whereas in the ξ direction (tangential coordinate) significantly less mesh points are utilized. η_{max} has been set at 10 and this defines an adequately large value at which the prescribed boundary conditions are satisfied. ξ_{max} is set at 1.0 for this flow domain. Mesh independence is therefore achieved in the present computations. The computer program of the algorithm is executed in MATLAB running on a PC. The method demonstrates excellent stability, convergence and consistency, as elaborated by Keller (1970).

4. RESULTS AND DISCUSSIONS

Comprehensive solutions have been obtained and are presented in Figs. 3 -20. The numerical problem comprises two independent variables (ξ,η), two dependent fluid dynamic variables (f,θ) and seven thermo-physical and body force control parameters, namely $\mathbf{Pr}$, $\mathbf{S_f}$, $\mathbf{S_T}$, β, $\mathbf{f_w}$, ξ and γ. In the present computations, the following default parameters are prescribed (unless otherwise stated): *Pr = 0.71, S_f = 0.5, S_T = 1.0, β = 1.0, f_w =*

0.5, ξ = 1.0 and $\gamma = 60^{\circ}$.

In Figs. 3 - 4, the influence of velocity slip parameter on velocity and temperature distributions is illustrated. Dimensionless velocity component (Fig. 3) at the wall is strongly increased with an increase in slip parameter, S_f. There will be a corresponding increase in the momentum (velocity) boundary layer thickness.
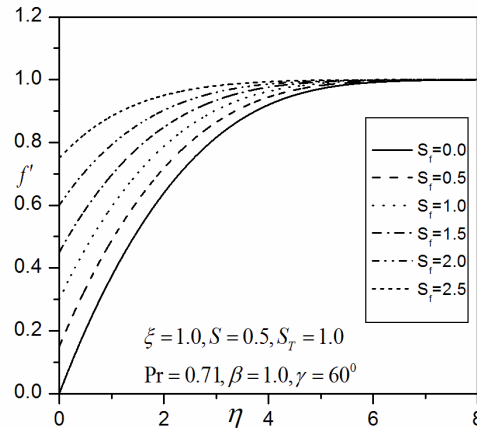
Fig. 3. Influence of S$_f$ on the Velocity.

The influence of S_f is evidently more pronounced closer to the inclined plate surface ($\eta = 0$). Further from the surface, there is a transition in velocity slip effect, and the flow is found to be accelerated markedly. Furthermore the acceleration near the wall with increasing velocity slip effect has been computed by Crane and McVeigh (2010) using asymptotic methods, as has the retardation in flow further from the wall. The switch in velocity slip effect on velocity evolution has also been observed for the case of a power-law rheological fluid by Ajadi *et al.* (2009). Fig.4 indicates that an increase in velocity slip parameter significantly enhances temperature in the flow field and thereby increases thermal boundary layer thickness enhances. This will result therefore in the transport of more thermal energy from the inclined plate surface to the Casson fluid and will therefore accentuate heat transfer to the fluid, as noted also by Wang (2007).
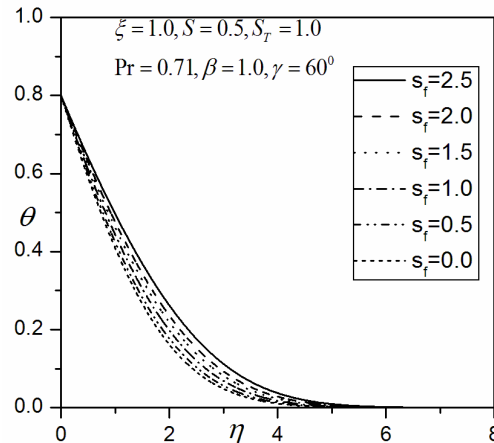
Fig. 4. Influence of S$_f$ on the temperature.

Temperature profiles consistently decay monotonically from a maximum at the inclined plate surface to the free stream. All profiles converge at large value of radial coordinate, again showing that convergence has been achieved in the numerical computations. A similar pattern of thermal response to that computed in Fig 4. for a wide range of velocity slip parameters has been noted by Aziz (2010) who has indicated also that temperature is enhanced since increasing velocity slip parameter decreases shear stresses and this permits a more effective transfer of heat from the wall to the fluid regime.

In Figs. 5 - 6, the variation of velocity and temperature with the transverse coordinate (η), with increasing thermal slip parameter S_T is depicted. The response of velocity is strongly decreased for all locations in the radial direction. The peak velocity accompanies the case of no thermal slip ($S_T = 0$). The maximum deceleration corresponds to the case of strongest thermal slip ($S_T = 3$).
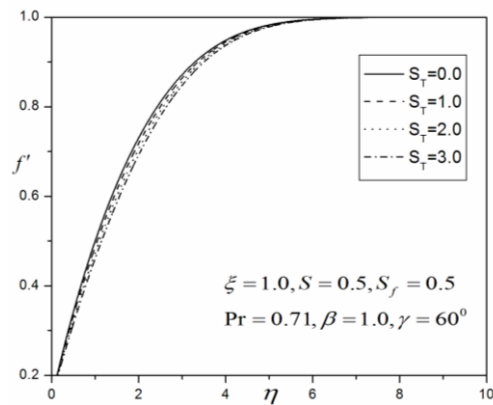
Fig. 5. Influence of S_T on the velocity.

Temperatures (Fig. 6) are also strongly depressed with increasing thermal slip. The maximum effect is observed at the wall.
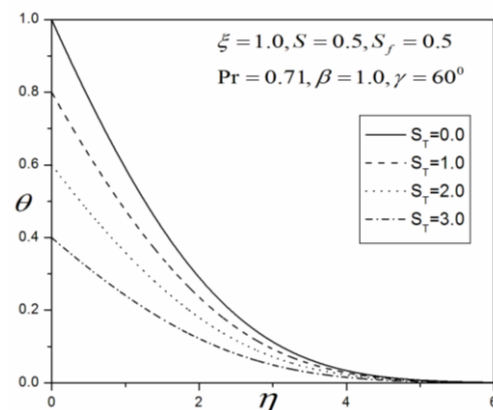
Fig. 6. Influence of S_T on the temperature.

The numerical computations correlate well with the results of Larrode *et al.* (2000) who also found that temperature is strongly lowered with increasing thermal slip and that this is attributable to the decrease in heat transfer from the wall to the fluid regime, although they considered only a Newtonian fluid.

In Figs. 7 - 8, depict the influence Casson fluid parameter, β on velocity and temperature profiles. An increase in β implies a decrease therefore in yield stress of the Casson fluid. This effectively facilitates flow of the fluid i.e. accelerates the boundary layer flow close to the inclined plate surface, as demonstrated by Fig. 7.
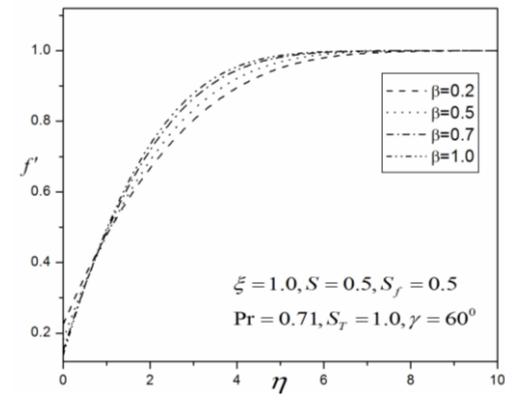

Fig. 7. Influence of β on the velocity.

Since the Casson parameter is also present in the wall boundary condition, the acceleration effect is only confined to the region close to the inclined plate surface. Further from this zone, the velocity slip factor, S_f will exert a progressively reduced effect and an increase in Casson parameter,β, will manifest with a deceleration in the flow.
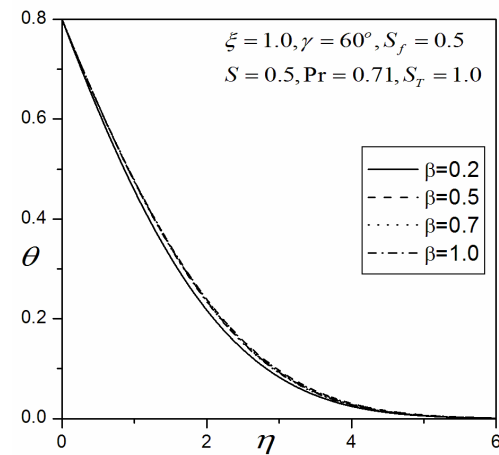

Fig. 8. Influence of β on the temperature.

Overall however the dominant influence of β, is near the wall and is found to be assistive to momentum development (with larger β values the fluid is closer in behaviour to a Newtonian fluid and further departs from plastic flow) Only a very small increase in temperature is observed with an enhancement in Casson fluid parameter, as shown in Fig. 8. The Casson parameter does not arise in the thermal boundary layer equation (11), nor does it feature in the thermal boundary conditions. The influence on temperature field is therefore experienced indirectly via coupling of the thermal eqn. (11) with the momentum eqn. (10). Similar

behaviour to the computations shown in Figs. 7 and 8, has been observed by Attia and Sayed-Ahmed (2010) who also observed acceleration in Casson fluid flow near a curved surface, and additionally by Mustafa *et al.* (2011) who also observed an elevation in velocities near the wall and a slight reduction in temperatures throughout the boundary layer regime.
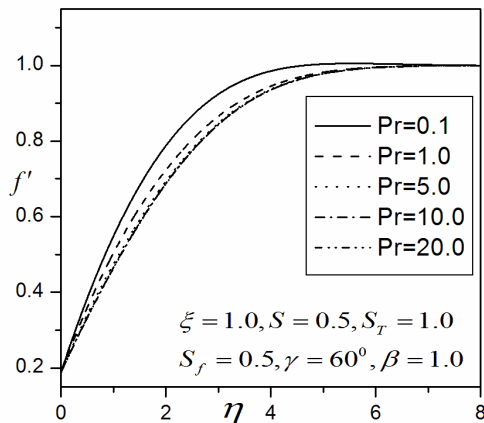

Fig. 9. Influence of Pr on the velocity.

Figs. 9 - 10, present the effect of Prandtl number (*Pr*) on the velocity and temperature profiles along the radial direction, normal to the inclined plate surface. Prandtl number embodies the ratio of viscous diffusion to thermal diffusion in the boundary layer regime. It also expresses the ratio of the product of specific heat capacity and dynamic viscosity, to the fluid thermal conductivity. When Pr is high, viscous diffusion rate exceeds thermal diffusion rate. An increase in *Pr* from 0.1 through 1.0, 5.0, 10.0 to 20.0, is found to significantly depress velocities (Fig. 9) and this trend is sustained throughout the regime i.e. for all values of the radial coordinate, η. For *Pr* <1, thermal diffusivity exceeds momentum diffusivity i.e. heat will diffuse faster than momentum. Therefore for lower *Pr* fluids (e.g. *Pr* = 0.01 which physically correspond to liquid metals), the flow will be accelerates whereas for greater *Pr* fluids (e.g. *Pr* = *1*) it will be strongly decelerated, as observed in fig. For *Pr* =*1.0*, both the viscous and energy diffusion rates will be the same as will the thermal and velocity boundary layer thicknesses. This case can be representative of food stuffs e.g. low-density polymorphic forms of chocolate suspensions, as noted by Steffe (2001).

Temperature is found to be strongly reduced with increasing Prandtl number. For the case of *Pr* = 0.1, the decay is almost exactly *linear*. For larger *Pr* values, the decay is found to be *increasingly monotonic*. Therefore for lower thermal conductivity fluids, lower temperatures are observed throughout the boundary layer regime.

Figs. 11 - 12, illustrate the influence of wall transpiration on the velocity and temperature functions with radial distance, η. With an increase in suction (f_w> 0) the velocity is clearly increased i.e. the flow is accelerated. Increasing suction

causes the boundary layer to adhere closer to the flow and destroys momentum transfer; it is therefore an excellent control mechanism for stabilizing the external boundary layer flow on the plate. Conversely with increased blowing i.e. injection of fluid via the inclined plate surface (f_w< 0), the flow is strongly accelerated i.e. velocities are increased. As anticipated the case of a solid inclined plate (f_w= 0) falls between the weak suction and weak blowing cases. Peak velocity is located, as in the figures described earlier, at close proximity to inclined plate surface. With a decrease in blowing and an increase in suction the peaks progressively displace closer to the inclined plate surface, a distinct effect described in detail in several studies of non-Newtonian boundary layers (O. Anwar Bég,2012; Rashidi, 2012;Hayat,2012).
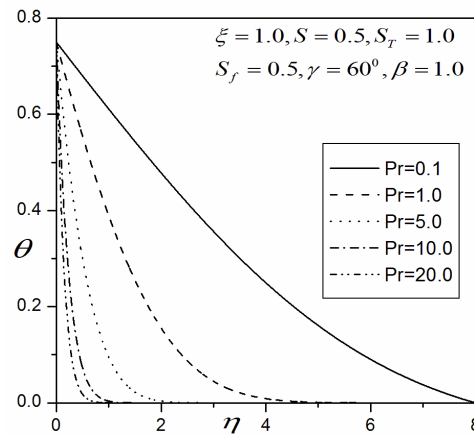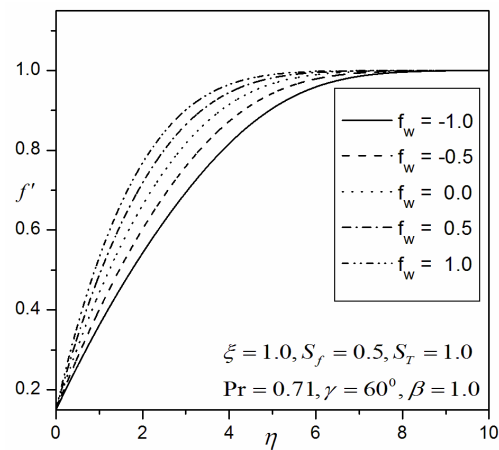

Fig. 10. Influence of Pr on the temperature.

Fig. 11. Influence of f_w on the velocity.

Temperature,θ, is also elevated considerably with increased blowing at the inclined plate surface and depressed with increased suction. The temperature profiles, once again assume a continuous decay from the inclined plate surface to the free stream, whereas the velocity field initially ascends, peaks and then decays in to the free stream. The strong influence of wall transpiration (i.e. suction or injection) on boundary layer variables is clearly highlighted. Such a mechanism is greatly beneficial in achieving flow control and regulation of heat and mass transfer characteristics in food processing
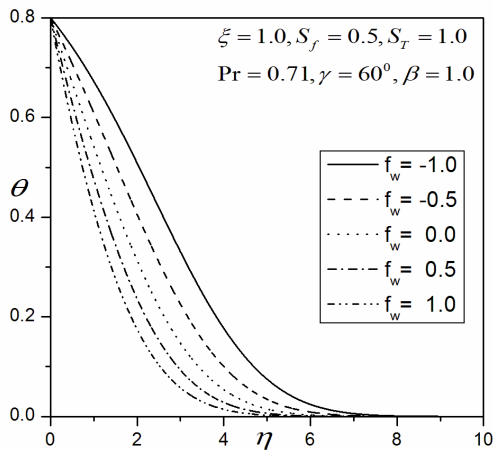
from a cylindrical geometry.

Fig. 12. Influence of f_w on the temperature.

Figs. 13 – 14 presents the variation of velocity and temperature fields with different transverse coordinate, ξ. In the vicinity of the inclined plate surface, velocity (f') is found to be maximized closer to the plate and minimized with progressive distance away from it i.e. the flow is decelerated with increasing ξ. Temperature (θ) is found to noticeably decrease through the boundary layer with increasing ξ values. Evidently the fluid regime is cooled most efficiently at the lower stagnation point and heated more effectively as we progress around the inclined plate periphery upwards towards the upper stagnation point.
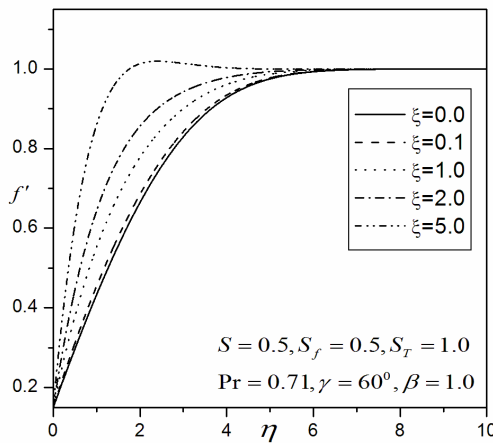

Fig. 13. Influence of ξ on the velocity.

These patterns computed for temperature and velocity evolution around the inclined plate surface are corroborated with many other studies including work on Newtonian convection from a cylinder by Wang (2007).

Figs. 15 - 16, the effects of plate inclination on the dimensionless velocity, temperature function with coordinate transverse to the plate (η) are illustrated. When $\gamma < 0$ *i.e.* negative plate inclination, in Figure 15, the velocity (f') is reduced at first *i.e.* flow is initially decelerated nearer the

plate surface; however further away it is accelerated. For the case of the vertical plate ($\gamma = 0$ degrees) and for positive inclination, velocities are always monotonic distributions and no overshoot is present.
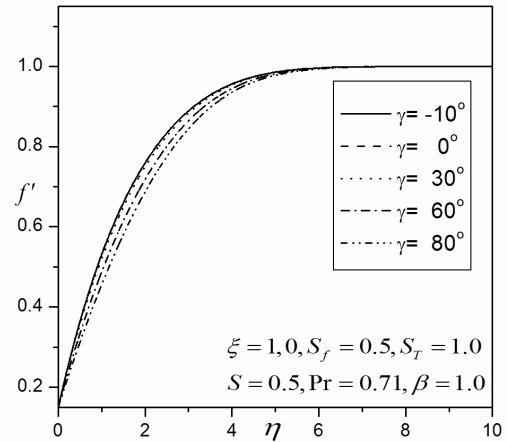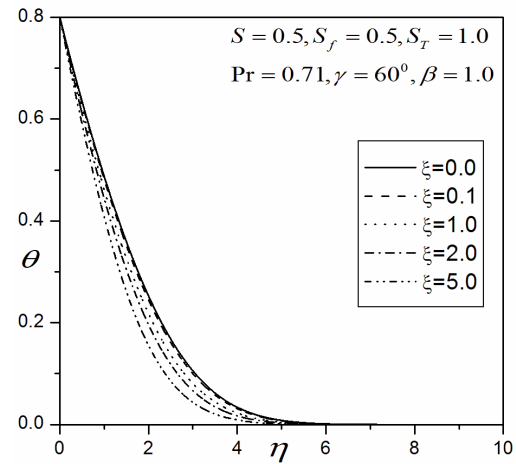

Fig. 15. Influence of γ on the velocity.

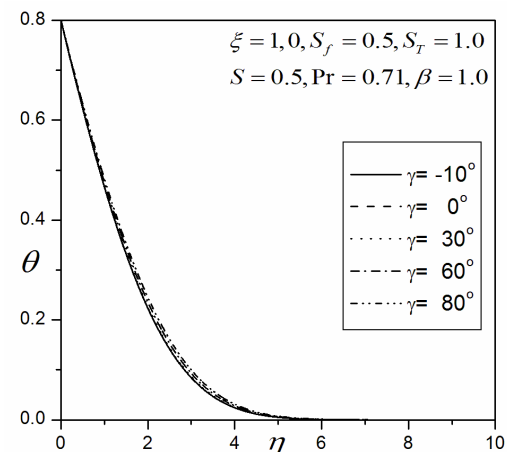
Fig. 14. Influence of ξ on the temperature.

Fig. 16. Influence of γ on the temperature.

With $\gamma > 0$ i.e. 30 degrees and 80 degrees, velocity is reduced i.e. flow is decelerated, largely owing to gravitational effects. Conversely in Figure 16, with negative plate inclination ($\gamma < 0$) the temperature

(θ) increases slightly for a vertical plate temperatures are greater than for the negatively inclined plate; temperatures are further increased marginally with positive inclination of the plate.

Figs. 17 - 18, show the effect of velocity slip parameter S_f on inclined plate surface shear stress (f'') and local Nusselt number (-θ') variation. In consistency with the earlier graphs described for velocity evolution, with an increase in S_f, wall shear stress is consistently reduced i.e. the flow is decelerated along the inclined plate surface.
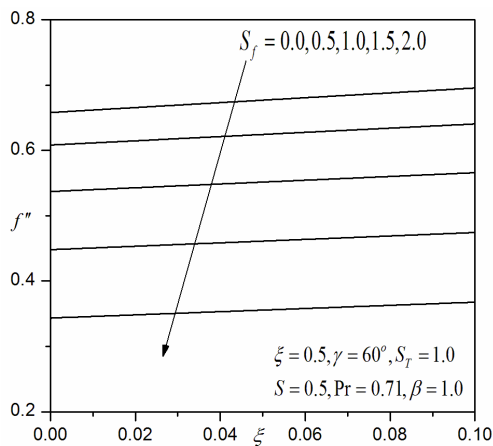

Fig. 17. Effect of S_f on the Skinfriction Coefficient results.

There is also a progressive migration in the peak shear stress locations further from the lower stagnation point, as wall slip parameter is increased. The impact of wall slip is therefore significant on the boundary layer characteristics of Casson flow from an inclined plate. With an increasing S_f, the local Nusselt number is also considerably decreased and profiles are generally monotonic decays.

Figs. 19 - 20, show the effect of thermal slip parameter S_T and non-Newtonian Casson fluid parameter on dimensionless local Nusselt number, respectively. Increasing S_T is found to decrease the local Nusselt number.
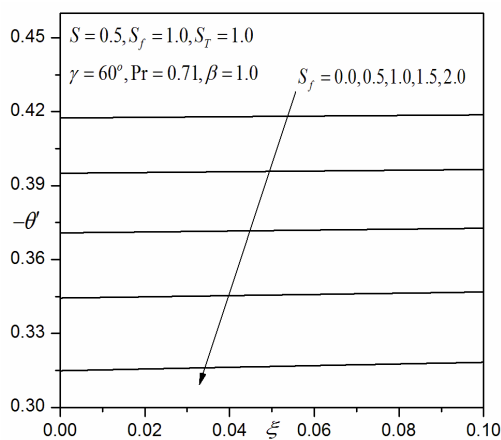

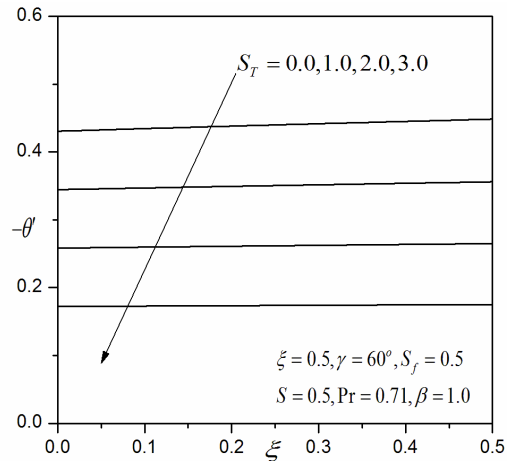**Fig. 18. Effect of S_f on the Local Nusselt Number results.**

Fig. 19. Effect of S_f on the local Nusselt Number results.

For lower values of thermal slip, the plots are parabolic nature; however with S_T values greater than 1, the profiles lose their curvature and become increasingly linear in nature. This trend is maximized for the highest value of S_T (= 3.0) for which local Nusselt number is found to be almost invariant with transverse coordinate, ξ Local Nusselt number is conversely found to decrease slightly as Casson fluid parameter is increased. With increasing β values, less heat is transferred from the inclined plate surface to the fluid regime, resulting in lower temperatures in the regime external to the inclined plate and lower local Nusselt numbers, as observed in Fig. 20.
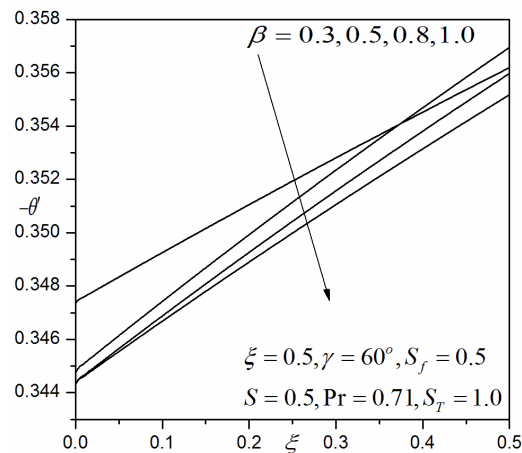

Fig. 20. Effect of β on the local Nusselt Number results.

Moreover, in order to verify the accuracy of present method, the analytical results obtained in the present work were compared with those available in the literature, obtaining an excellent agreement with those given in Wang (2008) and Kameswaran (2014) for particular values of suction/injection parameter f_w. It can also be noticed that for the values of $f_w < 0$ heat transfer decreases and increases for $f_w > 0$ as shown in Table 1.

Table 1 Comparison of −θ′(0) for different values of f_w when β→ ∞, Pr=0.71, S$_f$=S$_T$=γ=0

f_w	−θ′(0)		
	Wang (2008)	Kameswaran (2014)	Present study
-0.25	0.66857	0.6685728	0.66856
-0.5	0.50145	0.5014476	0.50145
-0.75	0.29376	0.2937625	0.29377
0	0.811301	0.8113013	0.8113
0.1	0.86345	0.8634517	0.86345
0.2	0.91330	0.9133028	0.91333

5. CONCLUSIONS

Numerical solutions have been presented for the transport phenomena i.e. combined heat and flow of Casson rheological fluid external to an inclined plate, with suction/injection effects and velocity/thermal slip. The model has been developed to simulate foodstuff transport processes in industrial manufacturing operations. A robust, extensively-validated, implicit finite difference numerical scheme has been implemented to solve the transformed, dimensionless velocity and thermal boundary layer equations, subject to physically realistic boundary conditions. The computations have shown that:

Increasing the velocity slip parameter, S_f, increases the velocity, temperature and skin friction but decreases the local Nusselt number. Increasing the thermal slip parameter, S_T, decreases velocity, temperature and the local Nusselt number throughout the boundary layer regime. Increasing the Casson fluid parameter, β, increases the velocity near the plate surface but decreases velocity further from the plate, and also fractionally increases the temperature throughout the boundary layer regime. Increasing Prandtl number, Pr, decelerates the flow and also strongly depresses temperatures, throughout the boundary layer regime. For positive inclination angle of the plate ($\gamma = 60°$), flow is accelerated, with thermal buoyancy force parameter (ξ) whereas temperature (θ) are reduced with increasing thermal buoyancy parameter, ξ . For negative and positive plate inclinations ($\gamma < 0$ and $\gamma > 0$), the flow is accelerated and decelerated respectively; for these plate orientations however the temperature functions are increased respectively.

The current study has been confined to steady-state flow i.e. ignored transient effects, thermal radiation heat transfer effects (Ahmed, 2012; Crane and A. G. McVeigh, 2010, Vasu et.al 2011). These aspects are also of relevance to rheological food processing simulations and will be considered in future investigations.

REFERENCES

Ahmed, N. (2012). Soret and Radiation effects on Transient MHD free convection from an impulsively started infinite verticle plate. *Journal of heat transfer* 134(6), 9.

Ajadi, S. O, A. Adegoke and A. Aziz (2009). Slip boundary layer flow of non-Newtonian fluid over a flat plate with convective thermal boundary condition. *Int. J. Nonlinear Science* 8, 300-306.

Anwar Beg, O. Ahmed Bakier, V. Ramachandra Prasad and Swapan Kumar Ghosh (2011) Numerical modelling of non-similar mixed convection Heat and Species Transfer along an inclined solar energy collector surface with cross diffusion effects. *World journal of Mechanics* 185-196.

Anwar Bég, O. and O. D. Makinde. (2011), Viscoelastic flow and species transfer in a Darcian high-permeability channel. *J. Petroleum Science and Engineering* 76, 93–99

Anwar Bég, O., J. Zueco and L. M. Lopez- Ochoa (2011). Network numerical analysis of optically thick hydromagnetic slip flow from a porous spinning disk with radiation flux, variable thermo physical properties, and surface injection effects.

Anwar Bég, O., K. Abdel Malleque and M. N. Islam (2012). Modelling of Ostwald-deWaele non- Newtonian flow over a rotating disk in a non- Darcian porous medium. *Int. J. Applied Mathematics and Mechanics* 8, 46- 67.

Attia, H. and M. E. Sayed-Ahmed (2010). Transient MHD Couette flow of a Casson fluid between parallel plates with heat transfer. *Italian J. Pure Applied Mathematics* 27, 19-38.

Aziz, A. (2010). Hydrodynamic and thermal slip flow boundary layers over a flat plate with constant heat flux boundary condition. *Communications in Nonlinear Science and Numerical Simulation* 15, 573-580.

Batra. R. L. and B. Das. (1992). Flow of Casson fluid between two rotating cylinders. *Fluid Dynamics Research* 9, 133–141.

Bird, R. B., G. C. Dai and B. J. Yarusso (1983). The rheology and flow of viscoplastic materials. *Rev. Chem. Eng*. 1, 1-83

Casson, N. (1959). A Flow equation for pigment oil-suspensions of the printing ink type. *Rheolgy of Disperse Systems (C. C. Mill, ed.)*, 84. Pergamon Press, London

Chemical Engineering Communications, 198, 360-384

Chen, T. S., C. F. Yuh and Moustsoglou (1980). Combined Heat and Mass Transfer in Mixed Convection along Vertical and Inclined Plates. *International Journal of Heat and Mass Transfer* 23(4), 527- 537.

Chhabra, R. P. (2014). Momentum and Heat transfer from a circular cylinder in Bingam Plastic fluids. *International journal of Heat and Mass Transfer* 70, 564-577.

Crane, L. J. and A. G. McVeigh (2010). Slip flow on a microinclined plate. *Z. Angew. Math. Phys* 61, 3, 579-582.

Dash, R. K., G. Jayaraman and K. N. Mehta (2000). Shear-augmented dispersion of a solute in a Casson fluid flowing in a conduit, *Annals of Biomed. Engg.* 28, 373-385.

Fujii, T. and H. Imura (1972). Natural- Convection Heat Transfer from a Plate with Arbitrary Inclination. *International Journal of Heat and Mass Transfer* 15(4), 755-764.

Hayat, T., I. Pop and A. A. Hendi (2012). Stagnation-point flow and heat transfer of a Casson fluid towards a stretching sheet, *Zeit. Fr. Natur.* 67, 70-76.

Inman, R. M. (1964). Heat transfer for laminar slip flow of a rarefied gas in a parallel plate channel or a circular tube with uniform wall temperature. *NASA Tech. Report, D-2213.*

Keller, H. B. (1970). A new difference method for parabolic problems. *J. Bramble (Editor), Numerical Methods for Partial Differential Equations, Academic Press, New York, USA*

Kierkus,W. T. (1968). An Analysis of LaminarFree Convection Flow and Heat Transfer about an Inclined Isothermal Plate. *International Journal of Heat and Mass Transfer* 11(2), 241-252.

Larrode, F. E., C. Housiadas and Y. Drossinos (2000). Slip-flow heat transfer in circular tubes. *Int. J. Heat Mass Transfer* 43, 2669-2680

Lee, S. L. and K. Hsu (1989). Interaction of Surface Suction/Blowing with Buoyancy Force on Mixed Convection Flow Adjacent to an Inclined Flat Plate. *International Journal of Heat and MassTransfer* 32(10), 1989-1991.

Molla, M. M. and M. A. Hossain (2006). Effects of chemical reaction, heat and mass diffusion in natural convection flow from an isothermal sphere with temperature dependent viscosity. *Int. J. Comput.-Aided Eng. Software* 23, 840–857.

Neofytou, P. (2006). Transition to asymmetry of generalised Newtonian fluid flows through a symmetric sudden expansion. *J. Non-Newtonian Fluid Mechanics* 133, 132-140.

Prasad, V. R., B. Vasu and O. Anwar Bég (2011). *Thermo-diffusion and Diffusion-thermo Effects on Boundary Layer Flows*, Lambert Academic Publishing, Saarbrucken, Germany.

Ramachandra Prasad, V., A. Subba Rao and O. Anwar Bég (2013). Flow and Heat Transfer of Casson Fluid from a horizontal Circular Cylinder with Partial Slip in non-Darcy porous Medium. *J Appl Computat Math* 2, 127.

Ramachandra Prasad, V., A. Subba Rao, N. Bhaskar Reddy, B. Vasu and O. Anwar Bég (2012). Modelling Laminar Transport Phenomena In A Casson Rheological Fluid From A Horizontal Circular Cylinder With Partial Slip. *Proceedings of the Institution of Mechanical Engineers.* Part E: *Journal of Process Mechanical Engineering* published

Rashidi, M. M., O. Anwar Bég and M. T. Rastegari (2012). A study of non-Newtonian flow and heat transfer over a non-isothermal wedge using the Homotopy Analysis Method. *Chemical Engineering Communication* 199, 231-256.

Shaw, S., P. V. S. N. Murthy and S. C. Pradhan (2010). The effect of body acceleration on two dimensional flow of Casson fluid through an artery with asymmetric stenosis. *Open Transport Phenomenon J.*, 2, 55-68.

Shaw, S., R. S. R. Gorla, P. V. S. N. Murthy and C. O. Ng (2009). Effect of stenosis on the Casson fluid flow through a bifurcated artery. *Int. J. Fluid Mechanics Research* 36, 43-63.

Sheu, W. J and M. C. Lin (1996). Thermal Ignition in Buoyancy-Driven Boundary Layer Flows along Inclined Hot plates. *International Journal of Heat and Mass Transfer* 39(10), 2187-2190.

Sparrow, E. M. and S. H. Lin (1962). Laminar heat transfer in tubes under slip-flow conditions. *ASME J. Heat Transfer* 84, 363-639.

Steffe, J. F (2001). *Rheological methods in Food Process Engineering*, 2nd edn, Freeman Press, Michigan, USA

Tripathi, D., O. Anwar Bég and J. Curiel-Sosa (2012). Homotopysemi-numerical simulation of peristaltic flow of generalised Oldroyd-B fluids with slip effects. *Computer Methods in Biomechanics Biomedical Engineering.*

Vasu, B., V. R. Prasad and N. Bhaskar Reddy (2011). Radiation and Mass Transfer Effects on Transient Free Convection Flow of a Dissipative Fluid past Semi-Infinite Vertical Plate with Uniform Heat and Mass Flux. *Journal of Applied fluid mechanics* 4(1), 15-26.

Wang, C. Y. (2007). Stagnation flow on a cylinder with partial slip-an exact solution of the Navier–Stokes equations. *IMA J. Applied Mathematics* 72, 271-277.

Wickern, G. (1991). Mixed Convection from an arbitrarily Inclined Semi-Infinite Flat Plate. The Influence of the Inclination Angle. *International Journal of Heat and Mass Transfer* 34(8), 1935-1945.

Yan, W. M. and C. Y. Soong (1995). Convective Heat and Mass Transfer along an Inclined Heated Plate with Film Evaporation. *International Journal of Heat and Mass Transfer* 38(7), 1261-1269.